BMC JOURNAL OF SCIENTIFIC RESEARCH
A Multidisciplinary Peer Reviewed Research Journal
ISSN: 2594-3421 (Print), 2773-8191 (Online)

Infrared Analysis of Dust Temperature and Mass Around PSR J0407+16 Using IRIS 60 and 100μm Data

Arun Adhikari, Nabin Upadhya Dhakal*, Manjeet Kunwar*, Nabin Bhusal, Manil Khatiwada and Rajendra Paudel

Central Department of Physics, Tribhuvan University, Kirtipur, Kathmandu, Nepal.
*Corresponding Author: nabinupadhyadhakal@gmail.com , manjeetkunwar04@gmail.com

Received: August 12, 2025, Accepted: Dec. 16, 2025
DOI: 10.3126/bmcjsr.v8i1.87919

Abstract

We examine the physical properties of a localized interstellar dust structure in the vicinity of the millisecond pulsar PSR J0407+16 using archival far-infrared data from the Improved Reprocessing of the IRAS Survey (IRIS) at 60 and 100 μm. Infrared flux maps were extracted from FITS images using Aladin v2.5, and pixel-by-pixel analyses were carried out with Python. The 60/100 μm flux ratio was used to calculate dust colour temperatures under the assumption of optically thin emission and a fixed dust emissivity index (β = 2). A modified blackbody approach was used to estimate dust masses. Using a Gaia EDR3 distance of 200 pc, the dust temperature was found to fluctuate within a narrow range of 21.42–22.64 K, with a mean value of 22.05 K. 1.57–2.08 MJy sr⁻¹ at 60 μm and 10.77–11.78 MJy sr⁻¹ at 100 μm are the equivalent flux densities. The overall dust mass of the building is determined to be 1.37 × 10^{28} kg (≈0.007 M⊙), indicating a gas mass of 2.74 × 10^{30} kg (≈1.44 M⊙) for a gas-to-dust ratio of 100:1. Spatial variations in flux, temperature, and mass show mild asymmetries, and an inverse temperature mass relation (R^2 = 0.86) suggests a thermally stable dust environment close to local thermodynamic equilibrium. These results demonstrate how effectively weak, quiescent dust forms in the interstellar medium may be probed using archival infrared data.

Keywords PSR J0407+16; Interstellar dust; Dust temperature; Dust mass estimation; Infrared astronomy.

Introduction

The interstellar medium (ISM), which is mostly composed of gas and a small but significant amount of solid dust grains, is a fundamental component of galaxies. Despite making up just around 1% of the total ISM mass, interstellar dust has a disproportionate role in regulating the physical, chemical, and radiative processes of galaxies (Draine 2003 & Li 2001). By scattering and absorbing light, these granules which are typically micron-sized interact extensively with stellar radiation, producing visual effects like extinction and reddening (Savage & Mathis 1979). Following absorption, the energy is released once more as thermal radiation, primarily at infrared (IR) wavelengths. Thermal emission from interstellar dust accounts for over 30% of the Milky Way's total illumination, which is essential for maintaining the

galaxy's radiative energy balance (Low et al. 1984; Draine 2003). Furthermore, dust complicates astronomical observations by dimming and reddening background sources, which must be corrected to accurately interpret optical and ultraviolet data (Lada 1985). Additionally, starlight can be polarised by aligned dust grains, revealing information on interstellar magnetic fields (Lazarian & Hoang 2015). IR observations are crucial for following dust-rich regions that are opaque at shorter wavelengths because cold dust emission is concentrated at far-infrared wavelengths. Consequently, infrared astronomy has become a powerful tool for studying the ISM. IR photons can directly study the properties of dust in diffuse cirrus structures and star-forming regions because they can travel through dense molecular clouds (Draine 2003). The launch of the Infrared Astronomical Satellite (IRAS) in 1983 marked a milestone as it produced the first all-sky survey between 12 and 100 μm. By demonstrating widespread cold dust emission across the galaxy, these discoveries greatly enhanced our understanding of the distribution of galactic dust (Low et al. 1984). These datasets were further improved by the Improved Reprocessing of the IRAS Survey (IRIS), which improved zodiacal-light subtraction and calibration, making them ideal for quantitative dust research (Miville-Deschênes & Lagache 2005). Because their extremely regular pulsed signals are altered by the intervening medium through dispersion, scattering, and Faraday rotation, pulsars offer useful probes of the ISM. These effects allow for accurate measurements of magnetic field structure and electron density along the line of sight (Cordes & Lazio 2002; Han 2010). According to (Ng et al. (2011)), the binary millisecond pulsar PSR J0407+16 has a long orbital period and a spin period of 25.7 ms. Unlike many newborn pulsars, it has no observable supernova remnant, which suggests that its surroundings are quite peaceful. As a result, rather than being greatly affected by recent explosive events, PSR J0407+16 is an excellent location to examine cold dust formations that might be the product of long-term interactions with the pulsar wind or remnants of its developed binary companion (Lorimer 2008).

The primary objective of this work is to describe the physical properties of a restricted dust structure at PSR J0407+16 using previous far-infrared IRIS data. Specifically, we utilise infrared flux analysis at 60 and 100 μm to compute the dust mass and colour temperature in the selected region. Statistical analyses are also used to examine the distribution of flux, temperature, and mass measurements, which provide insight into the thermal homogeneity of the dust environment. Deviations from Gaussian behaviour are examined to identify possible contributions from background or embedded sources. Through this focused examination, the current effort aims to improve our understanding of thermally stable dust formations associated with evolved star remnants using PSR J0407+16 as a reference instance.

Data Reduction and Methodology

The dusty environment surrounding PSR J0407+16 was examined using far-infrared pictures from the Improved Reprocessing of the IRAS Survey (IRIS) at wavelengths

of 60 and 100 µm (Miville-Deschênes & Lagache 2005). Isocontour borders were generated and flux maps from the pertinent FITS images were used to locate coherent emission features. Dust colour temperatures were calculated pixel by pixel using the 60/100 µm flux density ratio under the assumption of optically thin dust emission and a fixed spectral emissivity index of β = 2 (Reach et al. 1999). Using typical modified blackbody (graybody) emission models, dust masses were then calculated from the 100 µm flux (Reach et al. 1999; Bernard et al. 2005). The SkyView Virtual Observatory was used to identify an isolated far-infrared emission feature at PSR J0407+16. The ATNF Pulsar Catalogue was the source of the pulsar coordinates (Manchester et al. 2005). A gnomonic projection, a 500 × 500 pixel picture size, and histogram equalisation to improve contrast were used to analyse an initial 3° × 3° field centred on the pulsar across several infrared bands (12–100 µm). A compact emission structure with a diameter of around 0.5° was localised through successive zoom-ins to fields of 2°, 1.5°, and 1°. In line with a localised dust concentration, this structure displays an infrared flux pattern that is centrally concentrated and declines radially away (Bernard et al. 2005). Aladin software (version 2.5) was used to process the related FITS pictures, enabling contour-based analysis and systematic flux extraction (Bonnarel et al. 2000). Based on its geometric symmetry, peak brightness, and consistent coverage across all IRIS bands (12, 25, 60, and 100 µm), the final region of interest was centred at RA (J2000) = $04^{h}\ 09^{m}\ 03.25^{s}$ and Dec (J2000) = +15° 56′ 17.3″.

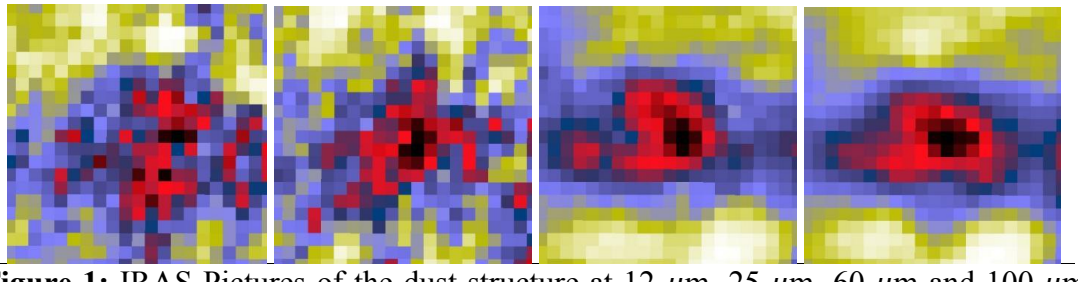

Figure 1: IRAS Pictures of the dust structure at 12 μm, 25 μm, 60 μm and 100 μm (left to right), each covering a 0.5° × 0.5° field centred at RA: $04^{h}\ 09^{m}\ 03.25^{s}$, DEC: +15° 56′ 17.3″. Cooler dust emission is indicated by brightness increasing with wavelength.

Temperature Estimation

Reduction of infrared data was done using the International Celestial Reference System (ICRS). To guarantee constant spatial sampling, isocontour levels of 49, 82, and 110 MJy sr^{-1} were specified in the 100 µm picture and superimposed onto the matching 60 µm image. Flux densities were derived from 400 pixels in a 0.5° × 0.5° field of view, 120 of which were inside the outermost contour. The appropriate 100 µm value and the 60 µm flux density were matched for every pixel. A linear regression analysis was then conducted to assess the correlation between the two

wavelengths and to characterise the thermal behaviour of the dust emission (Bernard et al. 2005). Dust colour temperatures (T_d) were derived from the 60/100 μm flux ratio under the assumptions of optically thin emission and a fixed emissivity index (β = 2), following the formalism of Reach et al. (1999) and Draine (2003). The temperature was calculated using the following expression, derived from the ratio of graybody functions:

$$\frac{S_{60}}{S_{100}} = \left(\frac{\nu_{60}}{\nu_{100}}\right)^{3+\beta} \frac{e^{h\nu_{100}/kT_d} - 1}{e^{h\nu_{60}/kT_d} - 1}$$

where S_{60} and S_{100} are the flux densities at 60 μm and 100 μm, respectively.

Dust Mass Estimation

Dust masses (M_d) were calculated using the prescriptions of Hildebrand (1983) and Young et al. (1993), (Hildebrand 1983; Young and al. 1993) which depend on the dust temperature, the distance to the source, and the adopted dust grain properties. The general expression for the dust mass is given by:

$$M_d = \frac{S_\nu D^2}{\kappa_\nu B(\nu, T_d)}$$

Where:

- $a = 0.1$ μm is the characteristic grain size,
- $\rho = 3000$ kg m^{-3} is the dust grain density,
- κ_ν is the grain emissivity (0.0010 m^2 kg^{-1} at 100 μm and 0.0046 m^2 kg^{-1} at 60 μm),
- $S_\nu = f_\nu \times 5.288 \times 10^{-19}$ W m^{-2} Hz^{-1}, where f_ν is the relative flux density extracted from the image.
- $B(\nu, T)$ is the Planck function evaluated at frequency ν and temperature T (Hildebrand 1983).

Given these values and constants, the dust mass equation simplifies to:

$$M_d = \frac{4\pi D^2 S_{100\mu\text{m}}}{\kappa_{100\mu\text{m}} B\left(\nu_{100\mu\text{m}}, T_d\right)}$$

This simplified form was used to compute the dust mass across all relevant pixels in the region of interest. To estimate the associated gas mass, a gas-to-dust mass ratio of 100:1 was adopted, following Henning et al. (1997) (Henning and al. 1997). The overall mass of the interstellar medium in the chosen area is roughly estimated by this assumption.

Result and Discussion

Infrared Flux Distribution: FITS images at 60 and 100 μm were analysed for a 0.5° × 0.5° region centred on PSR J0407+16. Isocontours defined from the 100 μm map were used to isolate a compact and well-defined emission structure, benefiting

from the higher contrast at longer wavelengths. Infrared flux densities extracted from this region show modest spatial variation, with values ranging from 1.57–2.08 MJy sr^{-1} at 60 μm and 10.77–11.78 MJy sr^{-1} at 100 μm are presented in Table 1. The relatively narrow flux ranges suggest a homogeneous emission environment, with no evidence for strong localised heating sources.

Table 1. Maximum, minimum, mean, range, standard deviation, and standard error of intensity of infrared flux in IRIS data.

Quantities	IRIS 60 μm (MJy sr^{-1})	IRIS 100 μm (MJy sr^{-1})
Fmax	2.08	11.78
Fmin	1.57	10.77
Fmean	1.82	11.37
Range	0.51	1.00
SD	0.10	0.28
SE	0.01	0.03

Dust Colour Temperature and Mass: The dust colour temperature was derived on a pixel-by-pixel basis using the 60 and 100 μm IRAS flux ratio, following standard approaches described by (Wood & Myers (1994), Schnee et al. (2005), and Dupac et al. (2003)). An emissivity index of $\beta = 2$ was assumed throughout. The dust temperature varies only slightly across the region, with values ranging from 21.42 ± 0.31 K to 22.64 ± 0.29 K and a mean temperature of 22.05 ± 0.01 K. The small temperature spread (~1.2 K) indicates a thermally stable dust structure that is weakly affected by external heating and close to local thermodynamic equilibrium. Dust mass was estimated from the 100 μm flux using the formulations of (Hildebrand (1983) and Young et al. (1993)). A distance of 200 pc, adopted from Gaia EDR3 measurements along the pulsar line of sight, was used for the mass calculation. A total dust mass of 1.37×10^{28} kg (≈0.007 M⊙) is obtained by adding up all the pixels in the chosen area. Assuming a standard gas-to-dust mass ratio of 100:1, the corresponding gas mass is 2.74×10^{30} kg (≈1.44 M⊙).

Table 2. Maximum, minimum, mean, range, standard deviation, and standard error of temperature of dust structure and isolated region.

Quantity	Dust Structure (K)
Tmax	22.64
Tmin	21.42
Tav	22.05
Range	1.22

SD	0.22
SE	0.01

Relationship Between Infrared Fluxes: To investigate the relationship between the relative flux densities at 60 μm and 100 μm, we plotted the flux values from the 100 μm FITS image along the X-axis and the corresponding flux values from the 60 μm FITS image along the Y-axis. As shown in Figure 2, the data exhibit a linear correlation between the infrared fluxes at the two wavelengths.

Table 3. Dust and Gas mass in the isolated area and dust structure.

Quantity	Dust Structure (kg)	Isolated Region (kg)
Mdust	1.37 × 1028	8.00 × 1028
Mgas	2.74 × 1030	1.60 × 1031

The best-fit linear regression is represented by the equation:

$$F(60\ \mu\text{m}) = 0.31 \times F(100\ \mu\text{m}) - 1.75$$

The slope of this relation (0.31) corresponds to the flux ratio between the two wavelengths and can be used to estimate the average dust color temperature. Based on this regression, the derived dust colour temperature is 25.87 K, calculated using an r^2 value of 0.66. However, this temperature differs from the one obtained using the pixel-by-pixel flux ratio method. The discrepancy is likely due to the relatively large y-intercept (-1.75) in the regression equation, which suggests deviation from the ideal linear model expected to pass through the origin (i.e., of the form $y = mx$). This discrepancy could be the result of background contamination or underlying non-linearities in the infrared flux measurements.

Table 4 The parameters of a linear fit.

Title	IRIS
Linear Equation	F(60) = 0.31 F(100) - 1.75
r^2 Coefficient	0.66
Slope	0.31
Average T_d	25.87 K

Temperature-Mass Relationship: Throughout the examined area, there is a clear inverse relationship between dust mass and temperature, with lower dust masses being associated with higher temperatures. The strength of this relationship is reflected by a coefficient of determination of $R^2 = 0.86$. Such behaviour is consistent with optically thin dust emission, where warmer material requires less mass to produce the observed infrared flux, and does not necessarily imply active dust destruction.

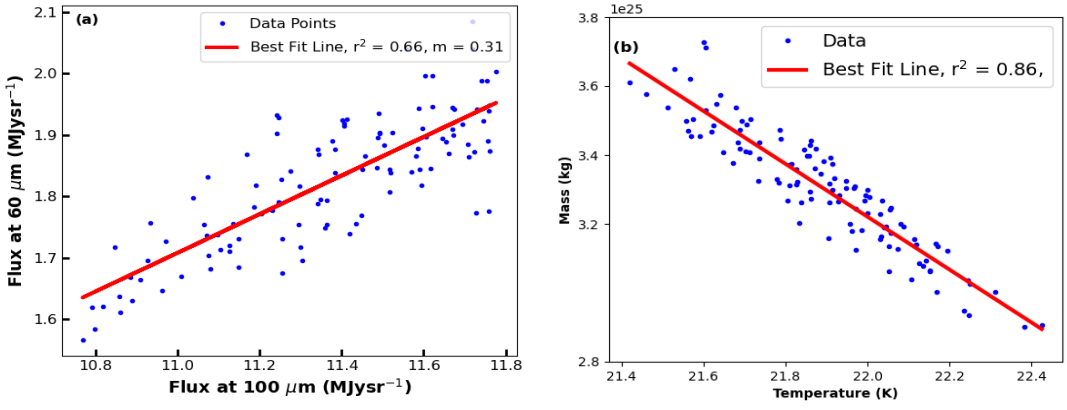

Figure 2. (a) Linear correlation between fluxes at 100 μm (X-axis) and 60 μm (Y-axis), with the best-fit line shown. The regression coefficient and slope are denoted by r and m, respectively. (b) Linear fit illustrating the inverse relationship between dust temperature and dust mass derived from IRIS data. The trend indicates that regions with higher dust temperature tend to have lower dust mass.

Colour Map of Infrared Flux, Temperature, and Mass: The spatial distributions of infrared flux at 60 and 100 µm, together with the derived dust colour temperature and mass, are shown as colour maps in Figure 3. The flux maps (Figures 3a and 3b) indicate systematically stronger emission at 100 µm than at 60 µm, consistent with radiation from cold dust. Regions of higher flux are concentrated toward the upper part of the field, with a gradual decrease toward the lower region, producing a clear north–south gradient.

On the other hand, the flux patterns are not directly followed by the dust temperature and mass distributions (Figures 3c and 3d). The upper-left and central-left sectors of the map are mostly home to cooler dust, whereas the lower-right and central-right sections show warmer places. While lower mass values predominate in the southern half of the field, the dust mass exhibits increased concentrations towards the top part, with a prominent maximum in the upper-right region. These discrepancies suggest that the spatial organisation of the dust is controlled by local changes in temperature and density rather than only flow.

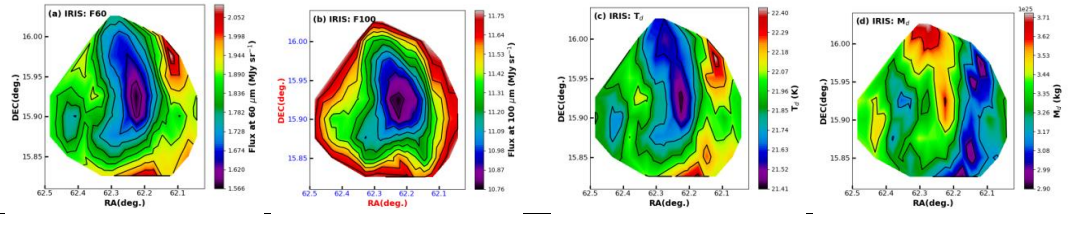

Figure 3: (a) infrared flux at 60 µm; (b) flux at 100 µm; (c) dust temperature; and (d) dust mass are displayed on colour maps with isocontours. On the X and Y axes,

respectively, are shown RA and DEC. Contour lines show areas of equal value, while colour bars show parameter scales. In the vicinity of PSR J0407+16, these maps show spatial changes in dust characteristics.

Gaussian Distribution of Flux, Temperature, and Mass: Gaussian distribution fits for the obtained dust temperature and dust mass, as well as the infrared fluxes at 60 and 100 μm, are shown in Figure 4. The observed values are displayed in each instance as histograms with normal probability density functions superimposed. A largely homogeneous and statistically well-behaved dust population is indicated by the dust temperature and dust mass distributions, which closely resemble a Gaussian profile.

The flux distributions, on the other hand, show a slight right-skewness at both wavelengths, indicating the existence of areas with increased infrared emission. Rather than inherent differences in the dust mass or temperature, this asymmetry is probably the result of localised contributions from embedded or background sources within the field. The identification of compact sources in astronomical catalogues like SIMBAD is consistent with this tendency.

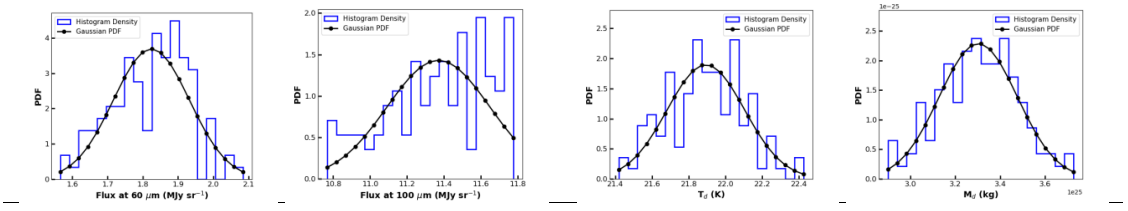

Figure 4. Physical parameters in the dust structure surrounding PSR J0407+16 are fitted using a Gaussian distribution. Histograms with overlaid Gaussian curves (black dotted lines) are shown for: (a) 60 μm flux, (b) 100 μm flux, (c) dust temperature, and (d) dust mass. While flux distributions exhibit right-skewness, most likely as a result of contributions from embedded sources like stars and young stellar objects, temperature and mass distributions closely resemble a normal distribution (SIMBAD catalogue).

Discussions

The derived dust temperatures (21.42–22.64 K) exhibit a narrow range across the region, indicating a thermally stable and weakly perturbed dust structure. Such uniformity suggests that the dust is close to local thermodynamic equilibrium and is not significantly influenced by strong external heating sources, including the pulsar itself. This behaviour is consistent with expectations for diffuse or moderately compact ISM structures in quiescent environments. At distances of a few hundred parsecs, the overall dust mass of 1.37×10^{28} kg ($\approx$0.007 M$\odot$) and the associated gas mass deduced using a conventional gas-to-dust ratio are typical of tiny ISM clumps. Mild asymmetries in the flux, temperature, and mass distributions are seen on spatial

maps; these asymmetries are probably caused by changes in background emission or local density rather than active dynamical processes. The emission's shared thermal origin is confirmed by a positive correlation between the 60 and 100 μm fluxes. Dust temperature and mass have an inverse relationship ($R^2 = 0.86$), which is consistent with optically thin dust emission, in which warmer locations contribute less mass for a given flux. Rather than being caused by actual temperature changes, the difference between temperatures obtained from pixel-by-pixel flux ratios and those deduced from linear regression most likely results from background offsets and non-linearities in the flux-flux relation. The interpretation of a reasonably homogeneous dust environment is supported by Gaussian analysis, which demonstrates that dust temperature and mass distributions are near to normal. On the other hand, localised contributions from embedded or background sources could be indicated by the flux distributions slight right-skewness. Overall, the findings point to a scenario where the dust structure close to PSR J0407+16 is a long-lived, stable ISM feature with little recent energetic disruption.

The dust structure surrounding PSR J0407+16 appears to be a stable and slightly disrupted interstellar feature based on the combined flux, temperature, and mass assessments. The concept of a quiescent dust environment is supported by the lack of severe temperature gradients or high flux boosts, which indicate little effect from the pulsar itself.

Conclusions

Using IRIS data at 60 and 100 μm, we have published a far-infrared analysis of a localised dust structure near the millisecond pulsar PSR J0407+16. With a mean value of roughly 22 K, the analysis shows a relatively narrow dust temperature range, suggesting that the dust is thermally stable and near local thermodynamic equilibrium. At distances of a few hundred parsecs, the calculated dust mass of 1.37×10^{28} kg ($\approx 0.007\ M_\odot$) and the inferred gas mass based on a typical gas-to-dust ratio are in line with expectations for small, quiet interstellar clouds. There is little evidence of a large external heating or dynamical disturbance in the spatial fluctuations in flux, temperature, and mass, indicating that the pulsar has little effect on the surrounding dust. An optically thin emission regime is further supported by the reported inverse connection between dust mass and temperature. All things considered, this work shows how valuable archival infrared surveys are for characterising subtle and stable dust formations in the interstellar medium when paired with contemporary research methods. The approach used here is easily adaptable to comparable situations surrounding other evolved star objects. For precise mass calculations, a distance of 200 pc based on Gaia EDR3 was utilised (Gaia Collaboration 2021). This method's successful use emphasises the necessity of statistical analysis and virtual observatory tools for conducting efficient study on dim infrared structures. This work provides a strong foundation for further research in the future. To further restrict the physical parameters, particularly the dust composition

and grain size distribution, data from infrared missions with greater angular resolution and broader wavelength coverage, like as AKARI, WISE, and Planck, should be employed in later research (Matsuura 2008).

Additionally, by modifying this methodological framework to conduct comparable comparative studies of dust patches associated with other classes of evolved stellar objects, such as white dwarfs, AGB stars, and supernova remnants, a more thorough understanding of how stellar evolution affects the properties and distribution of interstellar dust can be attained (Povich and Dishoeck 2014).

Acknowledgement: The authors thank Tribhuvan University's Central Department of Physics at Kirtipur, Kathmandu, Nepal, for providing the essential academic environment and institutional resources that enabled this study. We would like to thank the department's teachers and colleagues for their insightful suggestions and constructive criticism, which significantly contributed to the growth and enhancement of this work.

References

Bernard, J.-P., and et al. (2005). The IRIS Maps as Tracers of the Diffuse Cirrus. *Astronomy & Astrophysics* 424 (2): 787–97. https://doi.org/10.1051/0004-6361:20042454.

Bonnarel, F., and et al. (2000). The ALADIN Interactive Sky Atlas. *Astronomy & Astrophysics Supplement Series* 143 (1): 33–40. https://doi.org/10.1051/aas:2000331.

Cordes, J. M., and T. J. W. Lazio. (2002). NE2001.i. A New Model for the Galactic Electron Density. *The Astrophysical Journal* 576 (2): 942–54. https://doi.org/10.1086/341908.

Draine, B. T. (2003). Interstellar Dust Grains. *Annual Review of Astronomy and Astrophysics* 41: 241–89. https://doi.org/10.1146/annurev.astro.41.011802.094901.

Draine, B. T., and A. Li. (2001). Infrared Emission from Interstellar Dust: II. The MILKY WAY Dust Properties. *The Astrophysical Journal* 551 (2): 807–21. https://doi.org/10.1086/320144.

Dupac, X., and et al. (2003). The Cosmic Infrared Background. *Astronomy & Astrophysics* 404 (1): L11–14. https://doi.org/10.1051/0004-6361:20030588.

Gaia Collaboration. (2021). Gaia Early Data Release 3: Summary of the contents and survey properties. *Astronomy & Astrophysics* 649: A1. https://doi.org/10.1051/0004-6361/202039657.

Han, J. L. (2010). Pulsar Rotation Measures and the Galactic Magnetic Field. *Annual Review of Astronomy and Astrophysics* 48: 51–92. https://doi.org/10.1146/annurev-astro-081309-130940.

Henning, T., and et al. (1997). The Dust Content of the Interstellar Medium: A New Model. *Astronomy & Astrophysics* 322: 307–20.

Hildebrand, R. H. (1983). The Determination of Mass and Energy in the Interstellar Medium. *Quarterly Journal of the Royal Astronomical Society* 24: 267.

Lada, C. J. (1985). Star Formation and the Interstellar Medium. *Annual Review of Astronomy and Astrophysics* 23: 267–313. https://doi.org/10.1146/annurev.aa.23.090185.001411.

Lazarian, A., and T. Hoang. (2015). Dust Grain Alignment and Polarization of Starlight. *The Astrophysical Journal* 813 (2): 84. https://doi.org/10.1088/0004-637X/813/2/84.

Lorimer, D. R. (2008). Binary and Millisecond Pulsars. *Living Reviews in Relativity* 11: 8. https://doi.org/10.12942/lrr-2008-8.

Low, F. J., and et al. (1984). The Infrared Astronomical Satellite (IRAS) Mission. *The Astrophysical Journal Letters* 278: L19–22. https://doi.org/10.1086/184223.

Manchester, R. N., and et al. (2005). The Australia Telescope National Facility Pulsar Catalogue. *The Astronomical Journal* 129 (4): 1993–2006. https://doi.org/10.1086/428489.

Matsuura, M. (2008). Akari, Wise, and Planck Infrared Missions: A Comparative Study. *Publications of the Astronomical Society of Japan* 60: 489–502. https://doi.org/10.1093/pasj/60.sp2.S489.

Miville-Deschênes, M.-A., and G. Lagache. (2005). IRIS: A New Generation of IRAS Maps. *Astronomy & Astrophysics* 424 (2): 773–85. https://doi.org/10.1051/0004-6361:20042453.

Ng, C. Y., and et al. (2011). The Millisecond Pulsar J0407+16: An Eclipsing Binary with a Very Low Mass Companion. *The Astrophysical Journal* 729 (2): 136. https://doi.org/10.1088/0004-637X/729/2/136.

Povich, M. S., and E. F. van Dishoeck. (2014). Tracing the lifecycle of interstellar dust and gas. *The Astrophysical Journal* 781 (2): 122. https://doi.org/10.1088/0004-637X/781/2/122.

Reach, W. T., and et al. (1999). The Structure of the Galactic Interstellar Medium. *The Astrophysical Journal* 521 (1): 304–18. https://doi.org/10.1086/307525.

Savage, B. D., and J. S. Mathis. (1979). The Ultraviolet Interstellar Extinction Curve. *Annual Review of Astronomy and Astrophysics* 17: 73–111. https://doi.org/10.1146/annurev.aa.17.090179.000445.

Schnee, S., and et al. (2005). Warm Dust in the Small Magellanic Cloud. *The Astrophysical Journal* 634 (2): 1031. https://doi.org/10.1086/497184.

Wood, D. O. S., and P. C. Myers. (1994). Cold Dust in Star-Forming Regions. *The Astrophysical Journal* 420: 596. https://doi.org/10.1086/173595.

Young, J. S., and et al. (1993). The FCRAO Extragalactic Survey: A Study of the Cold Dust and CO Emission from a Sample of Nearby Galaxies. *The Astrophysical Journal Supplement Series* 86: 535. https://doi.org/10.1086/191807.